Optimisation of photopolymers for holographic applications using the Non-local Photo-polymerization Driven Diffusion model

Michael R. Gleeson,[1,*] Jinxin Guo,[2] and John T. Sheridan[2]

[1]*Department of Computer Science, National University of Ireland Maynooth, Maynooth, Co. Kildare, Ireland*
[2]*School of Electrical, Electronic and Mechanical Engineering, Communications and Optoelectronic Research Centre, The SFI-Strategic Research Cluster in Solar Energy Conversion, College of Engineering, Mathematical and Physical Sciences, University College Dublin, Belfield, Dublin 4, Ireland*
[*]*michael.gleeson@ucd.ie*

Abstract: An understanding of the photochemical and photo-physical processes, which occur during photopolymerization is of extreme importance when attempting to improve a photopolymer material's performance for a given application. Recent work carried out on the modelling of the mechanisms which occur in photopolymers during- and post-exposure, has led to the development of a tool, which can be used to predict the behaviour of these materials under a wide range of conditions. In this paper, we explore this Non-local Photo-polymerisation Driven Diffusion model, illustrating some of the useful trends, which the model predicts and we analyse their implications on the improvement of photopolymer material performance.

OCIS codes: (050.1950) Diffraction gratings; (050.7330) Volume gratings; (090.2890) Holographic optical elements; (090.2900) Optical storage materials; (160.5335) Photosensitive materials; (160.5470) Polymers.

References and links

1. M. R. Gleeson and J. T. Sheridan, "Non-local photo-polymerization kinetics including multiple termination mechanisms and dark reactions: Part I. Modelling," J. Opt. Soc. Am. B **26**(9), 1736–1745 (2009).
2. M. R. Gleeson, S. Liu, R. R. McLeod, and J. T. Sheridan, "Non-local photo-polymerization kinetics including multiple termination mechanisms and dark reactions: Part II. Experimental Validation," J. Opt. Soc. Am. B **26**(9), 1746–1754 (2009).
3. M. R. Gleeson, S. Liu, J. Guo, and J. T. Sheridan, "Non-Local photo-polymerization kinetics including multiple termination mechanisms and dark reactions: Part III. Primary Radical Generation and Inhibition," J. Opt. Soc. Am. B **27**(9), 1804–1812 (2010).
4. S. Liu, M. R. Gleeson, J. Guo, and J. T. Sheridan, "High intensity response of photopolymer materials for holographic grating formation," Macromol. **43**(22), 9462–9472 (2010).
5. J. Lougnot, P. Jost, and L. Lavielle, "Polymers for holographic recording: VI. some basic ideas for modelling the kinetics of the recording process," Pure Appl. Opt. **6**(2), 225–245 (1997).
6. J. T. Sheridan and J. R. Lawrence, "Nonlocal-response diffusion model of holographic recording in photopolymer," J. Opt. Soc. Am. A **17**(6), 1108–1114 (2000).
7. J. R. Lawrence, F. T. O'Neill, and J. T. Sheridan, "Adjusted intensity nonlocal diffusion model of photopolymer grating formation," J. Opt. Soc. Am. B **19**(4), 621–629 (2002).
8. T. Fäcke, F. Bruder, M. Weiser, T. Rölle, and D. Hönel, U.S. Patent No, US 2011/0065827 A1, (2011).
9. C. Ye and R. R. McLeod, "GRIN lens and lens array fabrication with diffusion-driven photopolymer," Opt. Lett. **33**(22), 2575–2577 (2008).
10. A. B. Villafranca and K. Saravanamuttu, "Diffraction rings due to spatial self-phase modulation in a photopolymerizable medium," J. Opt. A, Pure Appl. Opt. **11**(12), 125202 (2009).
11. K. Curtis, L. Dhar, L. Murphy, and A. Hill, *Future Developments, in Holographic Data Storage: From Theory to Practical Systems*, (Wiley 2010).
12. A. C. Sullivan, M. W. Grabowski, and R. R. McLeod, "Three-dimensional direct-write lithography into photopolymer," Appl. Opt. **46**(3), 295–301 (2007).

#149462 - $15.00 USD Received 20 Jun 2011; revised 15 Jul 2011; accepted 17 Jul 2011; published 24 Oct 2011

13. J. V. Kelly, M. R. Gleeson, C. E. Close, F. T. O'Neill, J. T. Sheridan, S. Gallego, and C. Neipp, "Temporal analysis of grating formation in photopolymer using the nonlocal polymerization-driven diffusion model," Opt. Express **13**(18), 6990–7004 (2005).
14. M. R. Gleeson, S. Liu, S. O'Duill, and J. T. Sheridan, "Examination of the photoinitiation processes in photopolymer materials," J. Appl. Phys. **104**(6), 064917 (2008).
15. M. R. Gleeson and J. T. Sheridan, "A review of the modelling of free-radical photopolymerization in the formation of holographic gratings," J. Opt. A, Pure Appl. Opt. **11**(2), 024008 (2009).
16. G. H. Zhao and P. Mouroulis, "Diffusion-model of hologram formation in dry photopolymer materials," J. Mod. Opt. **41**(10), 1929–1939 (1994).
17. J. T. Sheridan, M. R. Gleeson, C. E. Close, and J. V. Kelly, "Optical response of photopolymer materials for holographic data storage applications," J. Nanosci. Nanotechnol. **7**(1), 232–242 (2007).
18. T. Trentler, J. Boyd, and V. Colvin, "Epoxy resin photopolymer composites for volume holography," Chem. Mater. **12**(5), 1431–1438 (2000).
19. S. Liu, M. R. Gleeson, J. Guo, and J. T. Sheridan, "Modeling the Photochemical Kinetics Induced by Holographic Exposures in PQ/PMMA Photopolymer Material," J. Opt. Soc. Am. B (to be published).
20. M. R. Gleeson, J. T. Sheridan, F. Bruder, T. Rölle, H. Berneth, M-S. Weiser and T. Fäcke, are preparing a manuscript to be called "Analysis of the holographic performance of a commercially available photopolymer using the NPDD model."
21. J. H. Kwon, H. C. Hwang, and K. C. Woo, "Analysis of temporal behaviour of beams diffracted by volume gratings formed in photopolymers," J. Opt. Soc. Am. B **16**(10), 1651–1657 (1999).
22. J. R. Lawrence, F. T. O'Neill, and J. T. Sheridan, "Photopolymer holographic recording material," Optik (Stuttg.) **112**(10), 449–463 (2001).
23. S. Blaya, L. Carretero, R. F. Madrigal, M. Ulibarrena, P. Acebal, and A. Fimia, "Photopolymerization model for holographic gratings formation in photopolymers," Appl. Phys. B: Lasers Opt. **77**(6–7), 639–662 (2003).
24. L. Carretero, S. Blaya, R. Mallavia, R. F. Madrigal, A. Beléndez, and A. Fimia, "Theoretical and experimental study of the bleaching of a dye in a film-polymerization process," Appl. Opt. **37**(20), 4496–4499 (1998).
25. S. Gallego, M. Ortuño, C. Neipp, A. Márquez, A. Beléndez, I. Pascual, J. V. Kelly, and J. T. Sheridan, "Physical and effective optical thickness of holographic diffraction gratings recorded in photopolymers," Opt. Express **13**(6), 1939–1947 (2005).
26. G. Odian, *Principles of Polymerization 4th Edition* (Wiley, New York, 1991).
27. S. Liu, M. R. Gleeson, and J. T. Sheridan, "Analysis of the photoabsorptive behaviour of two different photosensitizers in a photopolymer material," J. Opt. Soc. Am. B **26**(3), 528–536 (2009).
28. M. R. Gleeson, J. V. Kelly, C. E. Close, F. T. O'Neill, and J. T. Sheridan, "Effects of absorption and inhibition during grating formation in photopolymer materials," J. Opt. Soc. Am. B **23**(10), 2079–2088 (2006).
29. S. Liu, M. R. Gleeson, D. Sabol, and J. T. Sheridan, "Extended model of the photoinitiation mechanisms in photopolymer materials," J. Appl. Phys. **106**(10), 104911 (2009).
30. A. Fimia, N. Lopez, F. Mateos, R. Sastre, J. Pineda, and F. Amatguerri, "Elimination of oxygen inhibition in photopolymer system used as holographic recording materials," J. Mod. Opt. **40**(4), 699–706 (1993).
31. M. R. Gleeson, D. Sabol, S. Liu, C. E. Close, J. V. Kelly, and J. T. Sheridan, "Improvement of the spatial frequency response of photopolymer materials by modifying polymer chain length," J. Opt. Soc. Am. B **25**(3), 396–406 (2008).
32. J. Guo, M. R. Gleeson, S. Liu, and J. T. Sheridan, "Non-local spatial frequency response of photopolymer materials containing chain transfer agents: Part I. Theoretical modelling," J. Opt. A, Pure Appl. Opt. (to be published).
33. J. Guo, M. R. Gleeson, S. Liu, and J. T. Sheridan, "Non-local spatial frequency response of photopolymer materials containing chain transfer agents: Part II. Experimental results," J. Opt. A, Pure Appl. Opt. (to be published).
34. H. M. Karpov, V. V. Obukhovsky, and T. N. Smirnova, "Generalized model of holographic recording in photopolymer materials," Semi Conduct. Phys. Quantum Electron. Optoelectron. **2**(3), 66–70 (1999).
35. M. Toishi, T. Tanaka, K. Watanabe, and K. Betsuyaku, "Analysis of photopolymer media of holographic data storage using non-local polymerization driven diffusion model," Jpn. J. Appl. Phys. **46**(6A), 3438–3447 (2007).
36. M. Toishi, T. Takeda, K. Tanaka, T. Tanaka, A. Fukumoto, and K. Watanabe, "Two-dimensional simulation of holographic data storage medium for multiplexed recording," Opt. Express **16**(4), 2829–2839 (2008).
37. R. R. A. Syms, *Practical Volume Holography* (Clarendon Press, Oxford, 1990).
38. I. Aubrecht, M. Miler, and I. Koudela, "Recording of holographic diffraction gratings in photopolymers: Theoretical modelling and real-time monitoring of grating growth," J. Mod. Opt. **45**(7), 1465–1477 (1998).
39. M. D. Goodner and C. N. Bowman, "Modeling primary radical termination and its effects on autoacceleration in photopolymerization kinetics," Macromol. **32**(20), 6552–6559 (1999).
40. C. E. Close, M. R. Gleeson, and J. T. Sheridan, "Monomer diffusion rates in photopolymer material. Part I. Low spatial frequency holographic gratings," J. Opt. Soc. Am. B **28**(4), 658–666 (2011).
41. C. E. Close, M. R. Gleeson, D. A. Mooney, and J. T. Sheridan, "Monomer diffusion rates in photopolymer material. Part II. High-frequency gratings and bulk diffusion," J. Opt. Soc. Am. B **28**(4), 842–850 (2011).

#149462 - $15.00 USD Received 20 Jun 2011; revised 15 Jul 2011; accepted 17 Jul 2011; published 24 Oct 2011

1. Introduction

Photopolymer materials and the photochemical kinetics associated with them [1–7] have been studied extensively in both academia and industry due to the growing interest in applications involving photopolymers [8–12]. In order to maximise the potential of these materials for various applications, the necessity of a physically comprehensive theoretical model of the effects which occur during photopolymerization is becoming ever more important [1–7,13–15]. The provision of such a model will enable potential trends in a material's performance to be recognized and utilized [16, 17]. This will allow simulations of various ratios of key material components to be made, yielding indications of the most suitable material compositions required to increase material performance.

In a recent set of publications by the authors [1–3], significant steps have been made towards achieving the development of such a tool. This Non-local Photo-polymerization Driven Diffusion (NPDD) model provides a comprehensive theoretical representation of the processes, which occur during free radical photo-polymerization. Thus enabling predictions to be made in a physically realistic way about the behaviour of a number of different photopolymer materials [1,2,8,18–20], which possess very different material characteristics. In this paper, we examine in detail some of the predictions made by this NPDD model and analyse their impact on photopolymer material development.

This paper is structured as follows. In Section 2 we briefly present the photochemical reactions in a flowchart format followed by the subsequent coupled differential equations which constitute the NPDD model. Section 3 examines the various predictions made by the theoretical model. Simulations are used in order to illustrate the relevant behaviour, followed by analysis of their significance in terms of material development. A conclusion is then provided in Section 4.

2. NPDD model

2.1 Photochemical processes

The photochemical processes which take place during photopolymerisation are extremely complex [5,13,15,16,21–26] and have been presented in detail elsewhere [1–3]. In order to save laborious repetition, a flowchart which succinctly summarises these processes is presented in Fig. 1. These photochemical reactions are the foundation of the coupled differential equations which constitute the NPDD model, described in Sub-section 2.2.

In the flowchart, *hv* indicates the energy absorbed from a photon [3,14,26], *Dye* is the ground state photosensitiser, $^{3}Dye^{*}$ is the excited triplet state of the photosensitiser [3,14,27], *CI* is the coinitiator or electron donor concentration, *Z* is the inhibitor concentration [3,28] and *M* is the monomer concentration. $R^{\bullet}$ represents the primary radical concentration, $HDye^{\bullet}$ signifies a radicalised dye which has abstracted a hydrogen from the co-initiator, and *Di-hydro* is the transparent form of the dye. $M_1^{\bullet}$ represents a chain initiator species and $M_n^{\bullet}$ represents a growing polymer chain of length *n*, with an active macroradical tip. The term '*Dead*' signifies the cessation of the growth of a propagating chain [26], while the term '*Scavenged*' indicates the removal of a primary radical [1–3,26].

#149462 - $15.00 USD Received 20 Jun 2011; revised 15 Jul 2011; accepted 17 Jul 2011; published 24 Oct 2011

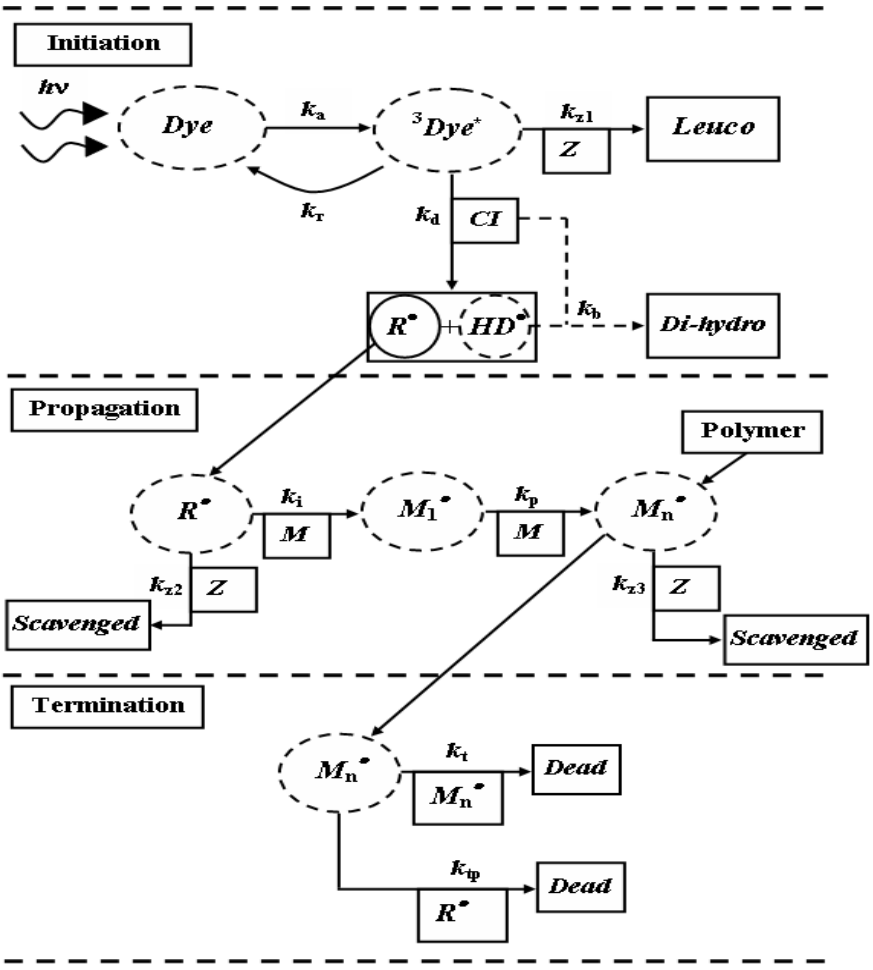

Fig. 1. Flowchart of the photochemical mechanisms, which take place during photopolymerisation.

The associated rates of reaction in Fig. 1 are; k_a (s^{-1}) the rate of production of excited state photosensitiser [3], k_r (s^{-1}) the rate of recovery or regeneration of photo-absorber [14,29], k_d ($cm^3mol^{-1}s^{-1}$) the rate of dissociation of the initiator and k_b ($cm^3mol^{-1}s^{-1}$) the rate of photosensitiser bleaching. k_i, k_p, k_t, and k_{tp} ($cm^3mol^{-1}s^{-1}$), are the rate constants of initiation, propagation, bimolecular termination and primary termination respectively [1–3,26]. k_{z1}, k_{z2} and k_{z3} ($cm^3mol^{-1}s^{-1}$) are the inhibition rate constants associated with an inhibitor reacting with excited dye molecules, primary radicals and macroradicals respectively [3,30].

As previously presented in [3], the rate of production of the excited state photosensitiser can be represented by $k_a = \phi \varepsilon d I_0'$ (s^{-1}), where ϕ (mol/Einstein) is the quantum efficiency of the reaction, ε (cm^2/mol) is the molar absorption coefficient and d (cm) is the photopolymer layer thickness. The intensity in Einsteins/cm^3s is given as $I_0' = \frac{T_{sf} B I_0}{d}\left(\frac{\lambda}{N_a hc}\right)$, where λ (nm) is the wavelength of incident light, N_a (mol^{-1}) is Avogadro's constant, c (m/s) is the speed of light, and h (Js) is Plank's constant. $B = 1 - e^{-\varepsilon A_0 d}$, is an absorptive fraction which determines a material's initial absorptive capacity and is dependent on the dye's initial concentration, A_0 (mol/cm^3), the molar absorptivity, ε, and the layer thickness, d. T_{sf} is a fraction which represents the amount of light lost from scatter and Fresnel reflections [14,23].

#149462 - $15.00 USD Received 20 Jun 2011; revised 15 Jul 2011; accepted 17 Jul 2011; published 24 Oct 2011

2.2 Coupled differential equations

In the case of holographic illumination of the photopolymer layer, there is a spatial distribution of irradiance which we assume to be co-sinusoidal and can be described as $I(x,t) = I_0'\left[1+V\cos(Kx)\right]$, where V is the fringe visibility and $K = 2\pi/\Lambda$, and Λ is the grating period. As a result of this spatial irradiance distribution, the photochemical reactions (Fig. 1) which occur within the photopolymer will have a temporal and spatial dependence [3], therefore inducing diffusion due to the presence of concentration gradients. The mechanisms which are presented in Fig. 1 can therefore be represented by a set of coupled differential equations which vary in time and space. Taking account of the mechanisms of initiation, propagation, termination and inhibition yields the following set of first-order coupled differential equations.

$$\frac{dDye(x,t)}{dt} = -k_a Dye(x,t) + k_r {}^3Dye^*(x,t), \tag{1}$$

$$\begin{aligned}\frac{d^3Dye^*(x,t)}{dt} &= k_a Dye(x,t) - k_r {}^3Dye^*(x,t) \\ &\quad - k_d {}^3Dye^*(x,t)CI(x,t) - k_{z1} {}^3Dye^*(x,t)Z(x,t),\end{aligned} \tag{2}$$

$$\frac{dCI(x,t)}{dt} = -k_d {}^3Dye^*(x,t)CI(x,t) - k_b HDye^\bullet(x,t)CI(x,t), \tag{3}$$

$$\frac{dHDye^\bullet(x,t)}{dt} = k_d {}^3Dye^*(x,t)CI(x,t) - k_b HDye^\bullet(x,t)CI(x,t), \tag{4}$$

$$\begin{aligned}\frac{dR^\bullet(x,t)}{dt} &= k_d {}^3Dye^*(x,t)CI(x,t) - k_i R^\bullet(x,t)u(x,t) \\ &\quad - k_{tp} R^\bullet(x,t)M^\bullet(x,t) - k_{z2} R^\bullet(x,t)Z(x,t),\end{aligned} \tag{5}$$

$$\begin{aligned}\frac{dM^\bullet(x,t)}{dt} &= k_i R^\bullet(x,t)u(x,t) - k_t\left[M^\bullet(x,t)\right]^2 \\ &\quad - k_{tp} R^\bullet(x,t)M^\bullet(x,t) - k_{z3} Z(x,t)M^\bullet(x,t),\end{aligned} \tag{6}$$

$$\begin{aligned}\frac{du(x,t)}{dt} &= \frac{d}{dx}\left[D_m(x,t)\frac{du(x,t)}{dx}\right] - k_i R^\bullet(x,t)u(x,t) \\ &\quad - \int_{-\infty}^{\infty} k_p M^\bullet(x',t)u(x',t)G(x,x')dx',\end{aligned} \tag{7}$$

$$\frac{dN(x,t)}{dt} = \int_{-\infty}^{\infty} k_p M^\bullet(x',t)u(x',t)G(x,x')dx' - \frac{d}{dx}\left[D_N(x,t)\frac{dN(x,t)}{dx}\right], \tag{8}$$

$$\begin{aligned}\frac{dZ(x,t)}{dt} &= \frac{d}{dx}\left[D_z(x,t)\frac{dZ(x,t)}{dx}\right] - k_{z1} {}^3Dye^*(x,t)Z(x,t) - k_{z2} Z(x,t)R^\bullet(x,t) \\ &\quad - k_{z3} Z(x,t)M^\bullet(x,t) + \tau_z\left[Z_0 - Z(x,t)\right].\end{aligned} \tag{9}$$

As discussed earlier, the non-uniform irradiance distribution used to record holographic gratings causes concentration gradients which lead to the diffusion of molecules. Equations (7–9) all consist of a one-dimensional standard diffusion term representing the diffusion of

#149462 - $15.00 USD Received 20 Jun 2011; revised 15 Jul 2011; accepted 17 Jul 2011; published 24 Oct 2011

their respective species, monomer, u (denoted earlier in the flow chart by M), polymer, N, and inhibitor, Z. Their diffusion coefficients (cm^2/s) are D_m, D_N and D_z respectively. It must be noted that in the analysis presented here, it is assumed that polymer diffusion effects are negligible, i.e., $D_N(x,t) = 0$.

In Eq. (9) we have also included a term to represent the replenishment of inhibiting oxygen into the material layer from the surrounding environment, where τ_z represents the rate of replenishment [3]. We note that it is assumed that the oxygen concentration which diffuses into an uncoverplated (not sealed) layer of the photopolymer can never be larger than the original concentration of dissolved oxygen present in the layer, Z_0 (mol/cm^3) and that this additive term is assumed to be spatially constant. The inhibition rate constants, k_{z2} and k_{z3}, will in general have different values (of reactivity) due to the differences in the relative molecular sizes reacting [26]. However in this analysis, for the sake of simplicity we treat $k_z = k_{z2} = k_{z3}$. Furthermore the reactivity of oxygen with the excited state form of the photosensitiser will be much lower, i.e. $k_{z1} << k_z$ and therefore we assume it is negligible in this analysis.

In Eqs. (7) and (8) we see the presence of the non-local material spatial response function $G(x,x')$ given by:

$$G(x,x') = \frac{1}{\sqrt{2\pi\sigma}} \exp\left[\frac{-(x-x')^2}{2\sigma}\right], \tag{10}$$

which represents the effect of initiation at location x' on the amount of monomer polymerized at location x [6,7]. In Eq. (10) σ is the constant non-local response parameter normalized with respect to the grating period, Λ. It is this non-local response parameter which determines the extent of nonlocal polymer chain growth and therefore a key factor in a photopolymer material's response at high spatial frequencies [31–33].

In previous work [6,7,16,21,26], it was assumed that polymerization responded instantaneously to changes in light intensity, i.e., that there was no temporal response and therefore no delay between initiation and polymerisation. This assumption results in an instantaneous cessation of polymerization when the exposure is stopped. However, it has been widely noted that under certain conditions a post-exposure grating amplification can be observed. This effect is caused by a combination of diffusion (material transport) and continued polymer chain growth post-exposure and is referred to as "*dark reactions*," or "post-exposure growth", [13,34–36]. These effects are more easily observed in the case of short exposures and therefore have a significant effect on applications where short exposure times are used, such as optical data storage.

In the case of the kinetic model presented here, there is no necessity to impose a non-local temporal response function into Eq. (10) as was done in [13]. During short exposures in a monomer rich environment, the time varying production of primary radicals by photon absorption, react with abundant monomer molecules to create macroradicals. These macroradicals, which initiate polymerization, are still present in the material post-exposure. As a result they will continue to react with the monomer present giving rise to further polymerization. This process will continue until all macroradicals are exhausted by termination or inhibitory reactions [1–3].

The kinetic model also accounts for the change in grating strength, which occurs when monomer diffusion becomes the dominant post-exposure mechanism (as seen in Fig. 3 in [13]) [2]. This post-exposure monomer diffusion results in two simultaneously occurring effects, which cause a change in the refractive index modulation. First, the diffusion of monomer out of the dark regions causes a change in the refractive index of that region, which can either increase or decrease depending on the relative refractive indices of the monomer and the background material (matrix, co-initiator, dye). Secondly, the diffusion of the monomer into the exposed bright regions of the interference pattern will subsequently cause a

#149462 - $15.00 USD Received 20 Jun 2011; revised 15 Jul 2011; accepted 17 Jul 2011; published 24 Oct 2011

change in the refractive index of that region. If there is a sufficient amount of unreacted macroradicals at this stage, an increase in polymerisation may occur due to the introduction of available monomer. However, as a result of the difference in the refractive indices between the monomer and polymer, some change in the refractive index of the region will occur. The combination of these two effects contributes to an overall change in the refractive index modulation post-exposure.

Since equations Eqs. (1–9), depend on the spatial distribution of the exposing intensity, they will all be periodic even functions of x and can therefore be written as Fourier series, $X(x,t) = \sum_{j=0}^{\infty} X_j(t)\cos(jKx)$, where X represents the species concentrations, Dye, $^3Dye^*$, CI, $HDye^\bullet$, $R^\bullet$, $M^\bullet$, u, N and Z. A set of first-order coupled differential equations can then be obtained in the same manner that was presented in [1–3] by gathering the coefficients of the various co-sinusoidal spatial contributions and writing the equations in terms of these time varying spatial harmonic amplitudes. These coupled equations can then be solved using the following initial conditions,

$$\begin{aligned} &Z_0(t=0) = Z_0, Dye_0(t=0) = Dye_0, CI_0(t=0) = CI_0, u_0(t=0) = U_0, \\ &Dye_{n>0}(t=0) = {}^3Dye^*_{n\geq 0}(t=0) = HDye^\bullet_{n\geq 0}(t=0) = CI_{n>0}(t=0) = 0, \text{ and} \\ &Z_{n>0}(t=0) = R^\bullet_{n\geq 0}(t=0) = M^\bullet_{n\geq 0}(t=0) = N_{n\geq 0}(t=0) = 0. \end{aligned} \quad (11)$$

As in previous analysis the Fourier series expansion of the monomer and polymer harmonics yield the non-local spatial response function represented by $S_i = \exp\left(-i^2K^2\sigma/2\right)$ [1,6,7].

Upon closer inspection of the above set of first order coupled differential equations, it can observed that the NPDD model takes account of; i) non steady state kinetics, ii) spatially non-local polymer chain growth, iii) temporal non-locality and dark reactions, iv) spatial and temporal variations in photon absorption and primary radical production (material nonlinearity), v) simultaneous inclusion of the effects of both primary, i.e. $R^\bullet$ - $M^\bullet$, and bimolecular, i.e. $M^\bullet$ - $M^\bullet$, termination, and vi) multiple inhibitory reactions.

Using the NPDD model proposed above, we will now examine some of its predictions of the behaviour of an acrylamide based polyvinylalcohol alcohol (AA/PVA) photopolymer material in an attempt to gain insight into optimising such a photopolymer. The kinetic rate constants used in the following simulations lie within physical reasonable ranges previously reported in the literature [1–3], in some cases unlikely extreme parameter values are used in order to illustrate potential trends.

3. Numerical predictions

A comprehensive review of the various photochemical models of free radical photopolymerization presented in the literature was recently published, highlighting the merits of each work and how these contributions have extended the understanding of the processes occurring during and post exposure [15]. The predominant emphasis of these works in terms of characterising material trends has been based on the response of the material to controllable physical recording conditions. These conditions include; the spatial frequency of the grating to be recorded [31–33], the recording dosage used, the thickness of the material layer [25], whether the grating is transmission or reflection type [37], is slanted or unslanted [37], and so on. To a lesser extent, some work characterising the photo-kinetic trends of a photopolymer have also been examined. One such example of this is the reduction of the nonlocal response of a material in order to improve a photopolymer's high spatial frequency response [6,7,31–33].

#149462 - $15.00 USD Received 20 Jun 2011; revised 15 Jul 2011; accepted 17 Jul 2011; published 24 Oct 2011

In this paper we attempt to highlight specific trends predicted by the NPDD model, presented in Section 2, based on the possible values of the rates of reaction of the photo-kinetic processes occurring during illumination. From these trends, information about the optimal kinetic rates can be obtained, indicating potential alternative chemical components characteristics which would improve a photopolymers performance.

3.1 Kinetic parameter variation

As the coupled differential equations presented in Section 2 generate solutions of the temporal and spatial variations in the concentrations of the constituent components of the photopolymer, we convert these values into volume fractions in the same manner as that previously presented in the literature [2,13,31,38]. Then using the Lorentz-Lorenz relation shown in Eq. (12) we relate these volume fractions and their associated refractive indices to the time varying refractive index modulation $n_1(t)$, where,

$$n_1(t) = \frac{\left(n_{dark}^2 + 2\right)^2}{6n_{dark}} \left[\varphi_1^{(m)}(t) \left(\frac{n_m^2 - 1}{n_m^2 + 2} - \frac{n_b^2 - 1}{n_b^2 + 2} \right) + \varphi_1^{(p)}(t) \left(\frac{n_p^2 - 1}{n_p^2 + 2} - \frac{n_b^2 - 1}{n_b^2 + 2} \right) \right]. \quad (12)$$

n_m represents the monomer refractive index, n_b the background refractive index, n_p the polymer refractive index and n_{dark} represents the overall refractive index of the photopolymer material before photo-polymerization. $\phi_1^{(m)}(t)$ and $\phi_1^{(p)}(t)$ are the time varying first harmonic volume fraction components of monomer and polymer respectively. In all simulations that follow, this procedure has been used to generate the refractive index modulation. The values for the refractive indices, volume fractions and concentrations of the components which constitute the AA/PVA photopolymer being examined are as presented in [1,13,31].

We will now examine the effect of varying specific rate constants to determine their effect on the performance of this AA/PVA photopolymer. In all simulations it is assumed that; $k_i = k_p$, $k_{tp} = 10 \times k_t$, $k_z = 1.0 \times 10^{11}$ cm^3/mols, $k_d = k_b = 1.6 \times 10^3$ cm^3/mols, $k_r = 1.2 \times 10^{-3}$ s^{-1}, $D_z = 1.0 \times 10^{-8}$ cm^2/s, $D_n = 0$ cm^2/s, $\varepsilon = 1.42 \times 10^6$ cm^2/mol, $\phi = 0.033$ mol/Einstein, $d = 100$ μm, $T_{sf} = 0.79$ and $S_1 = 0.9$. These estimated values are based on previous best fits obtained through numerical fitting of experimental growth curves of refractive index modulation and recording beam transmission and recovery curves [3,14]. All values lie within reasonable ranges presented in the literature [26,39–41].

Figure 2 shows a simulation of the saturated refractive index modulation, n_1^{sat}, of the AA/PVA photopolymer for various values of the propagation rate constant, k_p [26]. The simulation is generated for four different values of the monomer diffusion constant, $D_{m0} = 1\times10^{-10}$ cm^2/s (small dashed line), $D_{m0} = 1\times10^{-11}$ cm^2/s (dashed line), $D_{m0} = 5\times10^{-12}$ cm^2/s (long dashed line), and $D_{m0} = 1\times10^{-12}$ cm^2/s (longest dashed line) [40,41]. The gratings are recorded at a spatial frequency of 1500 lines/mm at an incident intensity of $I_0 = 1$ mW/cm^2. The bimolecular termination rate is fixed at $k_t = 6.0\times10^9$ (cm^3/mols) and therefore as mentioned above, the primary radical termination rate, $k_{tp} = 6.0\times10^{10}$ (cm^3/mols).

As can be seen from the figure, the optimum performance of the scenarios examined here for the AA/PVA photopolymer material, occur in the small dashed line case where the monomer diffusion coefficient is fastest at $D_{m0} = 1\times10^{-10}$ cm^2/s and where the propagation rate constant lies within the range of 5.0×10^7 - 1.0×10^8 cm^3/mols. An interesting prediction of this simulation is the reduction in the refractive index modulation achievable when the propagation rate is increased past a certain threshold. This makes logical sense as we are effectively increasing the polymerisation rate while maintaining the same monomer diffusion coefficient for each of the cases examined. As a result we are reducing the sinusoidal purity of the grating which causes a reduction in the refractive index modulation achieved. As expected, this effect is compounded further by a reduction in the monomer diffusion rate, see $D_{m0} = 1\times10^{-12}$ cm^2/s (longest dashed line). However as can be seen from the figure, an

#149462 - $15.00 USD Received 20 Jun 2011; revised 15 Jul 2011; accepted 17 Jul 2011; published 24 Oct 2011

increase in the monomer diffusion rate causes the limiting threshold of the propagation rate to increase.

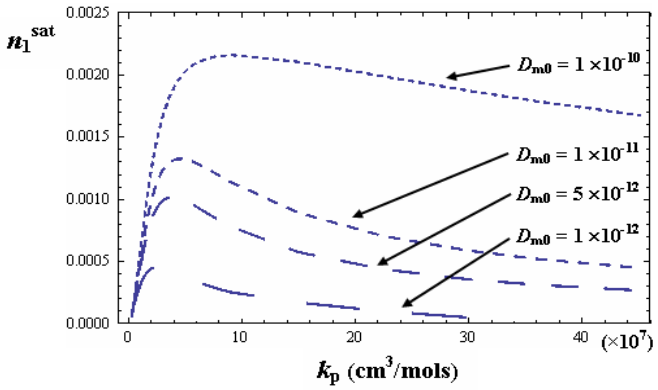

Fig. 2. Simulation of the saturated refractive index modulation, n_1^{sat}, for varying values of the propagation rate constant, k_p for a range of monomer diffusion coefficients, $D_{m0} = 1 \times 10^{-10}$ cm^2/s (small dashed line), $D_{m0} = 1 \times 10^{-11}$ cm^2/s (dashed line), $D_{m0} = 5 \times 10^{-12}$ cm^2/s (long dashed line), and $D_{m0} = 1 \times 10^{-12}$ cm^2/s (longest dashed line).

The observed physical effect is mirrored by those observed when there is a reduction in the reaction diffusion parameter, $R = D_{m0}K^2/F_0$, proposed by Zhao and Mouroulis [16], where D_{m0} represents the monomer diffusion coefficient, F_0 the polymerisation rate constant, (proportional to the recording intensity, I_0), and $K = 2\pi/\Lambda$, with Λ as the grating period. In this case, for the same monomer diffusion coefficient, an increase in the recording intensity causes a direct increase in the polymerisation rate constant, effectively reducing the reaction diffusion parameter, R. This effect is exacerbated by any reduction in the monomer diffusion coefficient. As has been reported repeatedly in the literature [6,7,16], a reduction in the value of R leads to a suppression of the amplitude of the first order refractive index modulation and an increase in the magnitude of higher grating harmonics. This ultimately causes a reduction in the overall grating strength, following the trend shown Fig. 2.

The predictions presented in Fig. 2 highlight the engineering capability provided through use of the NPDD model. As mentioned earlier, the majority of theoretical models presented in the literature can only predict the trends offered by changes in the physical recording conditions, such as the recording intensity or the spatial frequency of the grating recorded. However, the NPDD model presented here predicts the effects of changing both the photochemical and physical processes. In order to illustrate the compatibility and generality of the predictions of the NPDD model to the predictions of earlier theoretical models, Fig. 3a and 3b show the variation of the refractive index modulation at different spatial frequencies when the exposure intensity I_0 mW/cm^2 and monomer diffusion rate D_{m0} cm^2/s are changed respectively.

Figure 3a shows the saturated refractive index modulation, n_1^{sat}, over a range of spatial frequencies for various values of recording intensity, $I_0 = 0.5$ mW/cm^2 (long dashed line), $I_0 = 1.0$ mW/cm^2 (dashed line), $I_0 = 2.0$ mW/cm^2 (short dashed line), and $I_0 = 3.0$ mW/cm^2 (shortest dashed line). In this simulation the monomer diffusion coefficient was fixed at $D_{m0} = 1 \times 10^{-10}$ cm^2/s with $k_p = 2.6 \times 10^7$ and $k_t = 6.0 \times 10^9$. As can be easily seen from the figure, a reduction in the recording intensity causes an increase in the refractive index modulation achievable for all spatial frequencies examined. The low spatial frequency roll off can be observed as a consequence of insufficient monomer diffusion across the larger grating periods, which is also a result predicted using the reaction diffusion parameter discussed above. We also note the presence of the high spatial frequency cut-off which arises due to non-local effects, including polymer chain growth into the dark regions of the interference

#149462 - $15.00 USD Received 20 Jun 2011; revised 15 Jul 2011; accepted 17 Jul 2011; published 24 Oct 2011

pattern. In both Figs. 3a and 3b, the nonlocal response length was assumed to be $\sqrt{\sigma}$ = 25 nm.

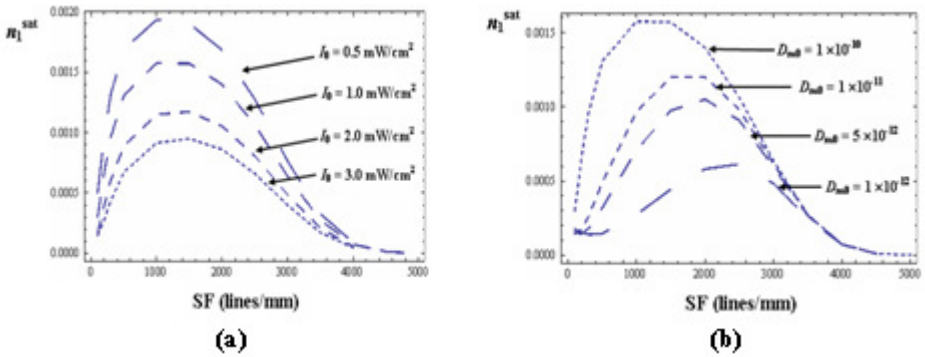

Fig. 3. (a) Spatial frequency response for varying exposure intensities, I_0 = 0.5 mW/cm^2 (long dashed line), I_0 = 1.0 mW/cm^2 (dashed line), I_0 = 2.0 mW/cm^2 (short dashed line), and I_0 = 3.0 mW/cm^2 (shortest dashed line); (b) Spatial frequency response for varying monomer diffusion coefficients, D_{m0} = 1×10^{-10} cm^2/s (small dashed line), D_{m0} = 1×10^{-11} cm^2/s (dashed line), D_{m0} = 5×10^{-12} cm^2/s (long dashed line), D_{m0} = 1×10^{-12} cm^2/s (longest dashed line).

Figure 3b shows the saturated refractive index modulation, n_1^{sat}, over a range of spatial frequencies for various values of monomer diffusion coefficients, with D_{m0} = 1×10^{-10} cm^2/s (small dashed line), D_{m0} = 1×10^{-11} cm^2/s (dashed line), D_{m0} = 5×10^{-12} cm^2/s (long dashed line), D_{m0} = 1×10^{-12} cm^2/s (longest dashed line). In this figure the recording intensity used was I_0 = 1.0 mW/cm^2. As expected we see that an increase in the monomer diffusion coefficient causes an increase in the achievable refractive index modulation over the spatial frequencies examined. We note that this is again consistent with an increase in the reaction diffusion parameter, R, which results in an increase in the refractive index modulation. Another trend which can be observed from the figure is the shift in the optimum performance of refractive index for each of the diffusion coefficients examined. In the longest dashed line scenario for D_{m0} = 1×10^{-12} cm^2/s we see that the maximum refractive index modulation achieved is at approximately 2500 lines/mm, whereas for the small dashed line case where D_{m0} = 1×10^{-10} cm^2/s the maximum refractive index modulation occurs at around 1200 lines/mm. This prediction is reasonable as there is a direct relationship between the monomer diffusion rate and the amount of monomer expected to diffuse from dark to bright regions.

Returning to our examination of the predictions of the model in relation to the photochemical processes, Fig. 4 shows the variation in saturated refractive index modulation, n_1^{sat}, of the AA/PVA photopolymer for various values of the bimolecular termination rate constant, k_t. These values all lie well within physically reasonable values [26]. As in the case of Fig. 2, the simulation is generated for four different values of the monomer diffusion constant, D_{m0} = 1×10^{-10} cm^2/s (small dashed line), D_{m0} = 1×10^{-11} cm^2/s (dashed line), D_{m0} = 5×10^{-12} cm^2/s (long dashed line), and D_{m0} = 1×10^{-12} cm^2/s (longest dashed line). The gratings are again recorded at a spatial frequency of 1500 lines/mm at an incident intensity of I_0 = 1mW/cm^2. In this case, the propagation and initiation rates are fixed at k_p = k_i = 2.6×10^7 (cm^3/mols).

As can be seen from the figure, the optimum performance of the scenarios examined here, occur in the small dashed line case where the monomer diffusion coefficient is fastest at D_{m0} = 1×10^{-10} cm^2/s and where the bimolecular termination rate constant lies within the range of 8.0×10^8 - 2.0×10^9 cm^3/mols. As expected, an increase in the bimolecular termination rate past some optimal value results in a reduction in the number of macroradicals available for chain propagation and hence results in the generation of a lower polymer concentration, leading to a drop in the refractive index modulation achieved. We also note that at relatively low values of

#149462 - $15.00 USD Received 20 Jun 2011; revised 15 Jul 2011; accepted 17 Jul 2011; published 24 Oct 2011

k_t, the effective rate of polymerisation will increase to some critical point after which there is a decrease in the magnitude of the first order of refractive index modulation and an increase in the magnitude of the higher grating harmonics amplitudes. This again reflects the behaviour predicted by the reaction diffusion parameter discussed above, and will ultimately cause a reduction in the overall grating strength as seen in Fig. 4.

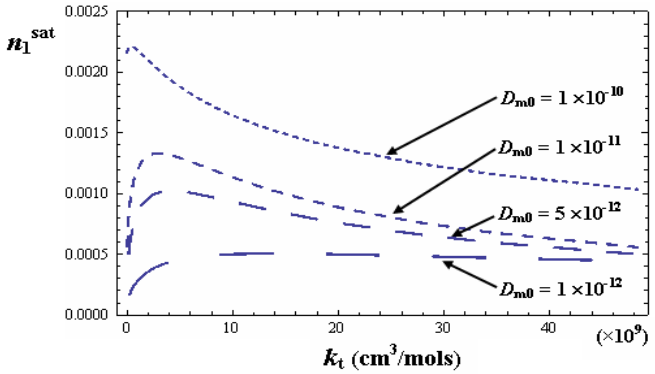

Fig. 4. Simulation of the saturated refractive index modulation for varying values of the bimolecular termination rate constant, k_t, for various values of the monomer diffusion coefficient, $D_{m0} = 1 \times 10^{-10}$ cm^2/s (small dashed line), $D_{m0} = 1 \times 10^{-11}$ cm^2/s (dashed line), $D_{m0} = 5 \times 10^{-12}$ cm^2/s (long dashed line), and $D_{m0} = 1 \times 10^{-12}$ cm^2/s (longest dashed line).

In order to further investigate the impact of the variations of these kinetic parameters on photopolymer performance, we now examine the behaviour of the rate of polymerisation, R_p, as a function of the monomer conversion, while simultaneously observing the time variation of the refractive index modulation, $n_1(t)$. The monomer conversion is defined as $\text{Conversion}(\%) = 100\left[1 - \frac{u_0(t)}{U_0}\right]$, where $u_0(t)$ is the zeroth harmonic of the monomer concentration and U_0 is the initial monomer concentration.

We begin by examining the effects of varying the propagation rate, k_p, while keeping the bimolecular termination rate fixed at $k_t = 6.0\times10^9$ cm^3/mols and the monomer diffusion coefficient fixed at $D_{m0} = 6.0\times10^{-11}$ cm^2/s.

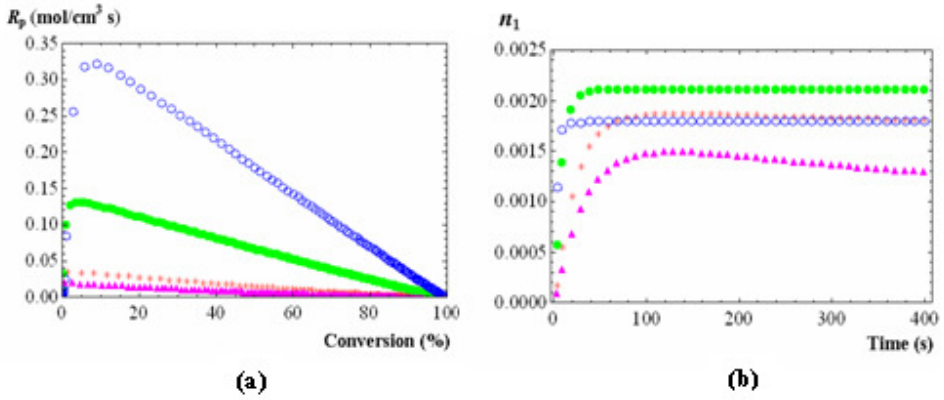

Fig. 5. (a) Simulation of the polymerisation rate, R_p, against monomer conversion and (b) simulation of growth curves of refractive index modulation, for varying propagation rates, $k_p = 1.5\times10^7$ cm^3/mols (purple triangle), $k_p = 2.6\times10^7$ cm^3/mols (red asterisk), $k_p = 1.0\times10^8$ cm^3/mols (green filled circle), $k_p = 2.6\times10^8$ cm^3/mols (blue empty circle).

#149462 - $15.00 USD Received 20 Jun 2011; revised 15 Jul 2011; accepted 17 Jul 2011; published 24 Oct 2011

Figure 5a shows the variation in the polymerisation rate as a function of the monomer conversion for; $k_p = 2.6 \times 10^8$ cm^3/mols (blue circles), $k_p = 1.0\times10^8$ cm^3/mols (green dots), $k_p = 2.6\times10^7$ cm^3/mols (red asterisk) and $k_p = 1.5\times10^7$ cm^3/mols (pink triangles). As there is a direct proportionality between the polymerisation rate and the propagation rate, $R_p = k_p [u_0][M_0^\bullet]$, the overall trend observed in the figure is reasonable. Increasing the propagation rate causes an increase in the polymerisation rate, while decreasing the propagation rate causes a decrease in the polymerisation rate and consequently a drop in the amount of monomer which is converted to polymer.

If we now examine Fig. 5b, which illustrates the corresponding refractive index modulation growth curves for the values of the propagation rate constants presented in Fig. 5a, we see that increasing the propagation rate from $k_p = 2.6\times10^7$ cm^3/mols (red asterisk) to $k_p = 1.0\times10^8$ cm^3/mols (green dots) causes an increase in the maximum refractive index modulation achieved. However, increasing the propagation rate further to $k_p = 2.6\times10^8$ cm^3/mols (blue circles), we see the expected increase in the polymerisation rate but we also observe a decrease in the refractive index modulation achieved. This is consistent with the predictions made in Fig. 2, where an increase in the propagation rate above a certain threshold ultimately reduces the sinusoidal purity of the grating formed and therefore causes a reduction in the refractive index modulation achieved.

Examining the effects of reducing the propagation rate below the critical threshold of optimal performance, i.e., $k_p = 1.5\times10^7$ cm^3/mols (pink triangles), sees a reduction in the polymerisation rate and a reduction in the magnitude of the refractive index modulation reached, as shown in Fig. 5b. This decrease in propagation rate causes a lower amount of polymer to be produced, which will automatically cause a reduction in the refractive index modulation achieved, see Eq. (12). Following the peak index modulation value reached there is a decay in the grating strength as the exposure time is increased further. This is attributed to the diffusion of monomer which is polymerised, but causing an increase in the magnitude of the higher grating harmonics, reducing the sinusoidal purity of the grating formed and hence a further reduction in the first harmonic of refractive index modulation.

We also note from Fig. 5a, that as the propagation rate is increased, the maximum polymerisation rate reached occurs at higher values of monomer conversions. This will have a significant effect on the refractive index modulation achievable as the mobility of monomer diffusing from the dark regions of the interference pattern will be reduced as the material viscosity increases in the exposed regions following increased monomer conversion.

Figures 6a and 6b show the effects of varying the bimolecular termination rate, k_t, on the polymerisation rate and the associated growth curves of refractive index respectively. In these figures the propagation rate is fixed at $k_p = 2.6\times10^7$ cm^3/mols and the monomer diffusion coefficient fixed at $D_{m0} = 6.0\times10^{-11}$ cm^2/s.

#149462 - $15.00 USD Received 20 Jun 2011; revised 15 Jul 2011; accepted 17 Jul 2011; published 24 Oct 2011

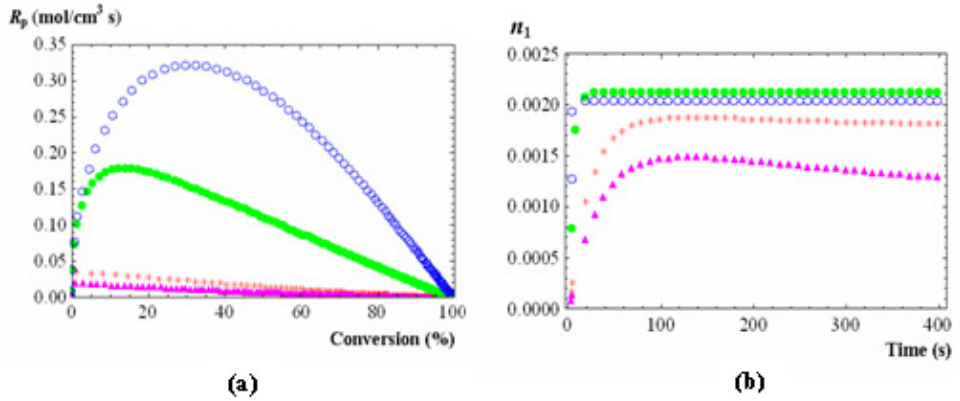

Fig. 6. (a) Simulation of polymerisation rate, R_p, against monomer conversion and (b) simulation of growth curves of refractive index modulation, for varying termination rates, k_t = 1.8×10^{10} cm^3/mols (purple triangle), k_t = 6.0×10^9 cm^3/mols (red asterisk), k_t = 1.5×10^8 cm^3/mols (green filled circle), k_t = 1.5×10^7 cm^3/mols (blue empty circle).

As expected, a reduction in the bimolecular termination rate will cause an increase in the polymerisation rate, while an increase in bimolecular termination will cause a reduction in the polymerisation rate. From Figs. 6a and 6b we see that reducing the bimolecular termination rate from k_t = 6.0×10^9 cm^3/mols (red asterisk) to k_t = 1.5×10^8 (green dots) results in an increase in the polymerisation rate and an increase in the refractive index modulation achieved. Reducing the bimolecular termination rate further to k_t = 1.5×10^7 cm^3/mols (blue circles) sees an increase in the polymerisation rate but a slight reduction in the refractive index modulation obtained. This is consistent with the predictions of Fig. 4 where an optimal region exists and reducing the bimolecular termination rate below this critical point will result in a decrease in the magnitude of the refractive index modulation due to an increase in the magnitude of the higher order grating components. Once again reflecting the prediction of the reaction diffusion parameter R [6,7,16], where increasing the polymerisation rate above a certain value will effectively reduce the grating strength.

If we now examine the case when the bimolecular termination rate is further increased to k_t = 1.8×10^{10} cm^3/mols (pink triangles), we see that the polymerisation rate is reduced and corresponding the maximum refractive index achieved is reduced. This follows the predictions presented in Fig. 4, where an increase in bimolecular termination leads to a reduction in the concentration of macroradicals available for polymerisation, resulting in an overall reduction in the polymer concentration and hence a reduction in grating strength. Following the maximum of the refractive index modulation reached for k_t = 1.8×10^{10} cm^3/mols (pink triangles) seen in Fig. 6b we see a decay in the growth curve. This decay is observed as a result of the low index monomer diffusing into the bright regions and as there is a depleted macroradical concentration, the monomer is not polymerised. Therefore this results in a decrease in the local refractive index and hence a reduction in the overall refractive index modulation.

Once again it must be noted that varying the photo-kinetic rate constants, in this case the bimolecular termination rate, causes the maximum polymerisation rate to occur at different monomer conversions. Therefore, as mentioned above, the effects of material viscosity will therefore play an important role in determining the maximum achievable grating strength.

4. Conclusions

With the constant development and increased complexity of theoretical models describing the photo-chemical effects taking place in photopolymers, it is often necessary to take a step back and analyse the various predictions being made. In this paper, the authors have examined, in

#149462 - $15.00 USD Received 20 Jun 2011; revised 15 Jul 2011; accepted 17 Jul 2011; published 24 Oct 2011

detail, some of the predictions of the most recent Non-local Photo-polymerisation Driven Diffusion model, which is a culmination of decades of work in the area of photopolymer modelling. As a result, this paper has illustrated some trends of practical importance when attempting to optimise the performance of a photopolymer material. As various types of monomer have diverse chemical and structural characteristics, knowledge of the characteristics required when choosing a monomer offers an informed choice to yield specific improvements in material performance. The implications of the predictions presented suggest that utilising a monomer with a large propagation rate constant and low bimolecular termination rate will produce a higher refractive index modulation. Furthermore, it is also desirable to have a monomer with high mobility, i.e., a fast diffusion rate, in order to increase the dynamic range of the photopolymer and to maximise the index modulation achievable. As highlighted in this paper, if the propagation rate is too large, or bimolecular termination rate is too small, the optimum refractive index modulation will not be obtained. These deleterious effects are compounded further by increased material viscosity as a result of polymerisation.

Acknowledgments

We acknowledge the support of the Irish Research Council for Science, Engineering and Technology through the Empower Postdoctoral research scholarship. We also acknowledge the support of Enterprise Ireland and Science Foundation Ireland through the national development plan.

#149462 - $15.00 USD Received 20 Jun 2011; revised 15 Jul 2011; accepted 17 Jul 2011; published 24 Oct 2011